Automatic detection of agricultural plastic greenhouses using deep learning and aerial RGB images

Davoud Omarzadeh[1], Mehran Alizadeh Pirbasti[*2], Hamed Bahrevar[3], Hoda Khalaghi[4], Gavin McArdle[2], Bahram Salehi[5]

[1] Institut d’Estudis Espacials de Catalunya (IEEC), Barcelona, Spain.
[2] School of Computer Science, University College Dublin, Dublin, Ireland.
[3] University of Tabriz, East Azerbaijan, Iran.
[4] Universitat Autònoma de Barcelona, Barcelona, Spain.
[5] State University of New York College of Environmental Science and Forestry (SUNY ESF), Department of Environmental Resources Engineering, Syracuse, USA.

Keywords: Agricultural plastic greenhouses, Aerial imagery, YOLOv11, U-Net, GeoAI, Environmental monitoring.

Abstract

Rapid urbanization in developing countries such as Iran has intensified pressure on agricultural land, highlighting the need for sustainable and efficient food production systems. Agricultural Plastic Greenhouses (APGs) have become a scalable alternative by enabling year-round cultivation and optimized land utilization. However, their rapid expansion necessitates continuous monitoring to evaluate structural integrity and environmental impacts, including soil degradation, plastic waste accumulation, and water consumption. This study presents a deep learning-based framework for the automated detection and condition assessment of APGs using 0.5 m resolution Google Earth imagery across four major agricultural regions in Tehran County: Pakdasht, Qarchak, Pishva, and Varamin. The proposed pipeline integrates YOLOv11 for precise APG segmentation with a U-Net architecture employing a MobileNetV2 backbone for classifying damaged and intact structures. Out of 158,912 analyzed image tiles, 6,835 contained APGs, covering an estimated area of 18.73 km^2. Among these, 1,863 damaged structures were identified, predominantly located in Pakdasht and Pishva. Around 20% of the annotated greenhouses were verified on-site, improving labeling reliability, and the relatively standardized design of APGs in Iran suggests the model could generalize to similar regions, with minor fine-tuning using local samples if necessary. GIS-based spatial analysis further delineated potential plastic waste risk zones, supporting targeted environmental management. Comparison with government statistics and Sentinel-2 imagery from 2021 and 2024 revealed a continued shift toward greenhouse farming in response to declining cropland availability. The proposed framework provides a scalable and replicable tool for periodic APG monitoring, facilitating data-driven policymaking and sustainable agricultural planning.

1. Introduction

The pace of urbanization in developing countries, such as Iran, has intensified pressure on arable land, resulting in the conversion of farmland into built-up areas and threatening local food security [Feizizadeh et al., 2022a, Ruel et al., 2017]. Plastic greenhouses have emerged as a practical solution for year-round cultivation, offering controlled environments and higher productivity per unit area [Chen et al., 2021, Baudoin and Von Zabeltitz, 2001]. In addition to monitoring greenhouse expansion, the prompt detection of damaged plastic greenhouse structures is essential for maintaining structural integrity, preventing plastic waste dispersion, and ensuring continued agricultural productivity. Beyond maintenance concerns, their accelerated expansion introduces environmental concerns, including plastic waste accumulation, soil degradation, and increased water demand that require continuous monitoring [Feng et al., 2021, Shi WeiMing et al., 2009, Gündoğdu et al., 2022]. By accurately identifying the location and area covered by greenhouses, stakeholders can implement targeted strategies to minimize these repercussions, preserving ecological balance and public health.

To tackle the challenges outlined, this research aims to develop a model for detecting agricultural plastic greenhouses (APGs) in two distinct scenarios. The first involves analyzing the quantitative aspects of APGs by extracting their spatial data, such as geographic location, surface area, shape, and spatial distribution patterns across the study region, while the second focuses on detecting and classifying damaged APGs to assess environmental contamination caused by plastic remnants and accurately pinpointing damaged structures to support farmers with timely maintenance. Both tasks will be addressed using remote sensing imagery, along with computer vision and deep learning techniques, which are further detailed in the subsequent sections of this paper.

In this study, a greenhouse is defined as “damaged” when high-resolution (0.5 m) imagery reveals clearly visible and spatially continuous structural deterioration, including partial or complete roof collapse, large-scale tearing or removal of the plastic covering, or significant deformation exposing underlying soil or vegetation. Minor perforations that are not reliably detectable at the available spatial resolution are excluded from this classification.

Specifically, deep learning techniques are employed for two main objectives. First, APGs are segmented with high precision using the You Only Look Once (YOLOv11) model. Second, a classification approach based on a Convolutional Neural Network (CNN) and MobileNetV2 is applied to classify damaged greenhouses. The overall process involves initially segmenting all greenhouses within the study area with high accuracy, followed by identifying damaged structures among the detected greenhouses using the classification model.

Field monitoring of APGs is often time-consuming, labor-intensive, and costly. To address this, remote sensing imagery

This contribution has been peer-reviewed. The double-blind peer-review was conducted on the basis of the full paper.
https://doi.org/10.5194/isprs-annals-XI-4-2026-53-2026

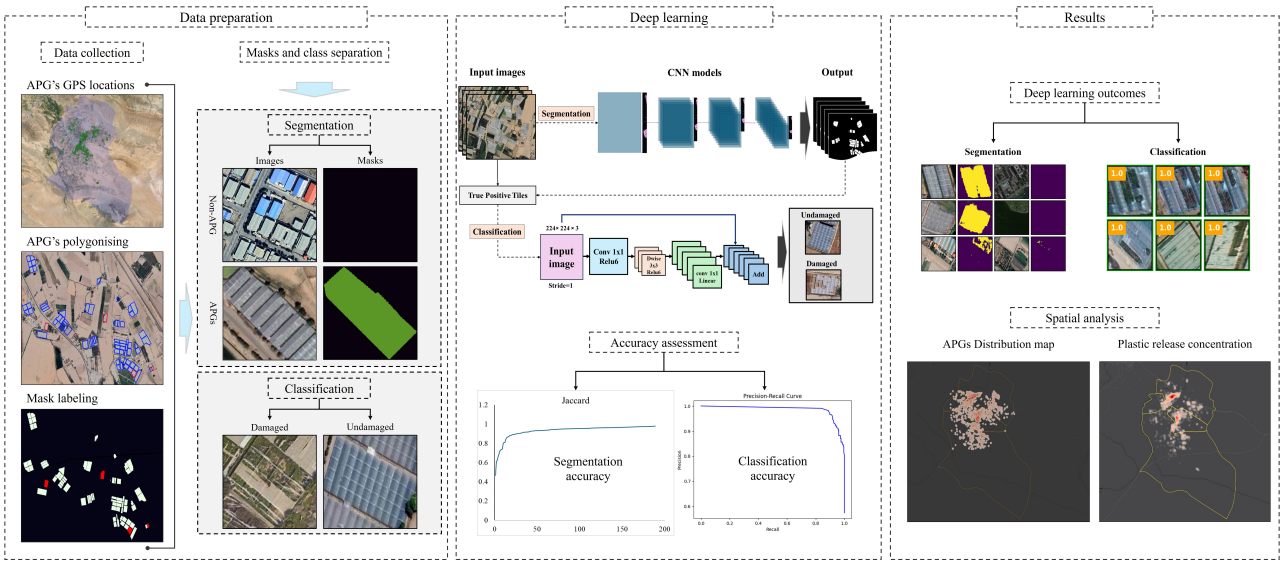

Figure 1. Overall workflow of the proposed framework for APG detection and damage assessment, including data acquisition, preprocessing, segmentation, classification, spatial analysis, and validation.

with various spatial and temporal resolutions plays a crucial role in efficient land surface mapping [Levin et al., 2007]. In recent years, advancements in computer vision and machine learning, particularly the evolution of deep learning algorithms, have unlocked new possibilities for extracting valuable insights from spatial datasets and remote sensing imagery [Omarzadeh et al., 2024, Feizizadeh et al., 2022b, Chen et al., 2018]. Therefore, land cover classification and segmentation are valuable tools for comprehending the spatial extent, dimensions, and composition of land occupied by natural or man-made materials. Building on this, automatic APG detection has been explored through different techniques, many of which have demonstrated notable success. For example, one of the most recent studies by [Tong et al., 2024] conducted a global assessment of greenhouse cultivation using satellite data and artificial intelligence, mapping 1.3 million hectares of greenhouse infrastructure as of 2019, significantly more than previously estimated. The study analyzed both large and small-scale greenhouses, revealing a notable increase in greenhouse cultivation in the Global South since the 2000s, with China alone accounting for 60% of the global coverage. While highlighting the potential of greenhouses to enhance food security, the research also raises concerns about the environmental and social implications of their rapid expansion, underscoring the need for comprehensive spatio-temporal datasets to support future studies. In another study, [Yang et al., 2017] used medium spatial resolution satellite data of Landsat and spectral indices for accurately detecting plastic greenhouses (APGs) in Shangdong Province, China. They achieved promising results with a kappa coefficient of 0.83 and an overall accuracy of 91.2%. Another study [Shi et al., 2019] adopted very high-resolution images from the GaoFen-2 satellite to monitor APGs. This approach integrates the Double Coefficient Vegetation Sieving Index (DCVSI), High-Density Vegetation Inhibition Index (HDVII), and Normalized Difference Vegetation Index (NDVI) to effectively distinguish plastic greenhouses from other land surfaces. Their outcomes yielded a mapping accuracy of 97.34%, demonstrating the method's robustness across different phenological stages and surrounding patterns. Similarly to our research context, [Koc-San, 2013], a study in Antalya, Turkey, used WorldView-2 satellite imagery with machine learning techniques to detect glass and plastic greenhouses. Supervised classifiers, including Maximum Likelihood (ML), Random Forest (RF), and Support Vector Machines (SVM), were applied. Among them, SVM achieved the highest accuracy (93.88%), followed by RF (91.73%), both outperforming ML significantly. This demonstrates the effectiveness of advanced classifiers, particularly SVM and RF, in greenhouse detection.

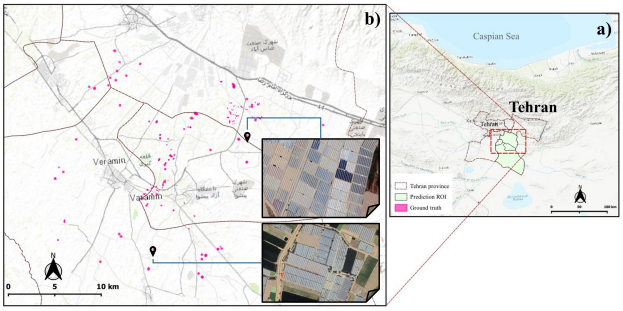

Figure 2. a) Represents the location of the study area within Tehran Province, and b) the distribution of collected ground truth within the study area.

Moreover, deep learning methodologies have been increasingly employed for diverse purposes, including the classification of urban features [Stewart et al., 2020, Qamar and Dobler, 2020], as well as land cover classification [Mboga et al., 2020, Gaetano et al., 2018]. Closer to our work, several studies have applied deep learning and aerial imagery to detect APGs. For instance, a study by [Chen et al., 2021] using Google Earth images implemented U-Net to identify and detect greenhouses from high-resolution aerial images, demonstrating the potential of deep learning in agricultural monitoring. Similarly, a research conducted by [Sun et al., 2021] employed a combination of deep learning techniques and Sentinel-2 satellite images to accurately map the distribution of plastic greenhouses, which significantly enhances the efficiency of agricultural land management. They achieved a kappa co-efficient of 0.81%. Additionally, [Jakab et al., 2021] focused on the application of semantic segmentation using deep learning models to detect APGs applying high-resolution RGB remote sensing images and convo-

This contribution has been peer-reviewed. The double-blind peer-review was conducted on the basis of the full paper.
https://doi.org/10.5194/isprs-annals-XI-4-2026-53-2026 | © Author(s) 2026. CC BY 4.0 License.

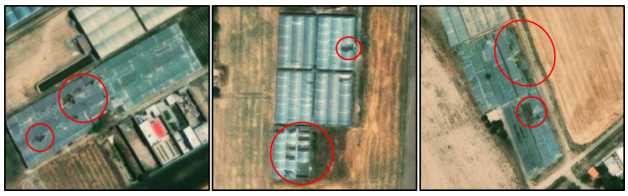

Figure 3. Samples of damaged APGs considered in this research

lutional neural networks. Based on their results, the VGG-11 backbone model resulted in an average accuracy of 79.2%, the much more complex DenseNet121 model showed a result of 79.1%, while the ResNet18-based model showed an average accuracy of 83.1%.

Although previous studies have been successful, they mainly focus on detecting plastic greenhouses without differentiating between damaged and intact structures. Most existing approaches treat greenhouses as homogeneous land-cover units and emphasize presence and absence mapping rather than structural condition assessment at the object level. Consequently, an integrated framework that combines high-precision segmentation, structural damage classification, and spatial environmental risk awareness remains largely unexplored in the current literature.

In addition, many of these studies overlook key spatial attributes such as the geographic location, size, shape, density, and spatial distribution patterns of greenhouses, which are essential for comprehensive spatial analysis, environmental assessment, and planning interventions. This limitation not only affects precise agricultural planning and structural assessment but also makes it difficult to monitor the presence and distribution of plastic remnants in the environment. In this research, we employ a multifaceted approach that integrates spatial analysis, statistical evaluation, and environmental considerations while also providing practical solutions for farmers to identify and repair damaged structures. By addressing these interconnected aspects, our methodology ensures both scientific robustness and real-world applicability.

In this research, we focus on the critical role of APGs in agriculture, food security, and environmental sustainability. Using high-resolution (0.5 meters) Google satellite imagery from 2024, which was exported using QGIS software, ensuring the original spatial resolution was preserved, we analyzed APG coverage in four locations, including Pakdasht, Qarchak, Pishva, and Varamin in Tehran County, Iran. Our approach introduces an object-level remote sensing pipeline that integrates instance segmentation and structural-condition classification to accurately detect and assess APGs.

We first apply YOLOv11 for segmentation, identifying areas covered by APG. Only the tiles containing APGs proceed to the next phase, where we use a Convolutional Neural Network (CNN) for classification. Specifically, we employ the U-Net architecture with a MobileNetV2 backbone to distinguish between damaged and undamaged greenhouses.

To ensure precise identification, we use pixel masks to differentiate APGs (value of 1) from other structures (value of 0). In addition, we employ Geographic Information System (GIS) tools to map the distribution of APGs and visualize potential areas that could be affected by plastic waste. This approach helps in environmental management by identifying potential sources of contamination and providing farmers with valuable information

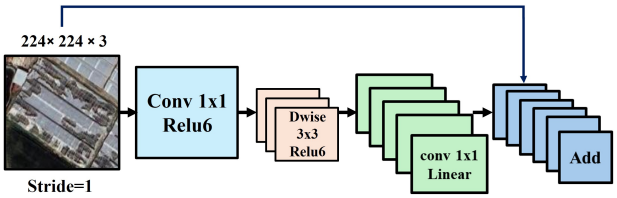

Figure 4. The classification pipeline begins with an input image processed by a 1×1 convolution with ReLU6 activation to expand feature channels. It then applies a depthwise separable 3×3 convolution to extract spatial features while minimizing computational complexity. The architecture includes inverted residuals, featuring an expansion layer, depthwise convolution, and a 1×1 linear convolution for effective feature transformation. Skip connections support residual learning, enhancing gradient flow and retaining important information. Finally, a classification layer determines whether the input image depicts a damaged or undamaged structure.

to maintain the greenhouse infrastructure. By optimizing agricultural practices in industrial greenhouse farming, our methodology contributes to environmental sustainability and improved food security.

The paper is structured as follows: In Section 2, we introduce our case study and describe the acquisition and preparation of the dataset, including satellite imagery, field-verified ground truth data, and the process of APG labeling and mask generation for model training. Section 3 presents the experimental outcomes, including segmentation and classification performance metrics, quantitative estimation of APG-covered areas, spatial distribution analysis, and identification of damaged structures potentially contributing to environmental contamination. Section 4 discusses the methodological strengths, limitations, and practical implications of the proposed framework, followed by concluding remarks.

To provide a clear overview of the proposed framework, Figure 1 illustrates the complete workflow of the study, including data acquisition, preprocessing, segmentation using YOLOv11-seg, damage classification using MobileNetV2, spatial analysis, and validation against official statistics.

2. Materials and Methods

In this study, the selected locations include four cities: Varamin (population 258839[1]), Pishva (67797), Pakdasht (271139), and Qarchak (265088). These cities are located 35 km southeast of Tehran, the capital of Iran. This area is known as the Greenhouse Plain in Iran (Figure 2).

According to the Tehran Province Management and Planning Organization, the province of Tehran, which is home to 9 million people, ranks first in the country in greenhouse area and production. It accounts for 20.7% of the greenhouse area of the nation and 30.4% of its greenhouse production, with the four cities examined in this study contributing to these figures [2]. This research utilizes two primary types of geospatial data: high-resolution satellite imagery and digitized geolocations of APGs. The following sections describe the data sources and preparation steps in detail.

[1] SData: Sharif Pajouh Data Processing
[2] Province Management and Planning Organization

This contribution has been peer-reviewed. The double-blind peer-review was conducted on the basis of the full paper.
https://doi.org/10.5194/isprs-annals-XI-4-2026-53-2026

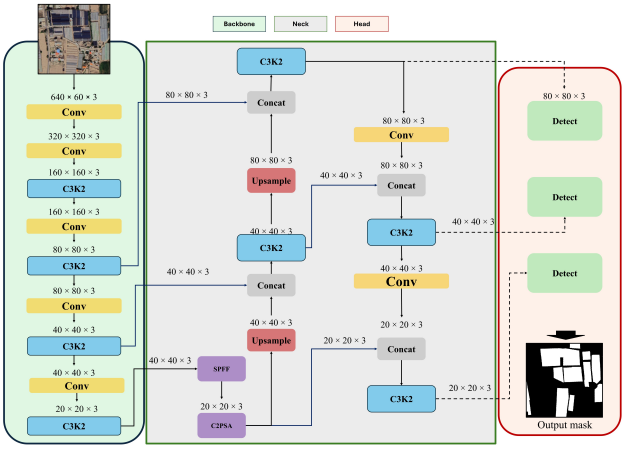

Figure 5. YOLOv11 Backbone, Neck, and Head with key blocks SPPF, C2PSA, and optimized C3K2 for efficient multi-scale feature extraction and detection.

This study applies remote sensing images obtained from Google Earth. The use of Google Earth images has become increasingly popular among remote sensing researchers across various fields. These applications include estimating urban vegetation analysis [Duhl et al., 2012], land use and land cover mapping [Pirbasti et al., 2024], forest studies [Ploton et al., 2012], and the mapping of plastic greenhouses [Chen et al., 2021]. In our region of interest, publicly accessible RGB images with a spatial resolution of 0.5 meters are available from the Airbus satellite [3] for the year 2024 [4]. Additionally, many researchers use Google Earth images as validation resources, which further motivates our decision to employ them in this study. To avoid losing the geographical information of the images, we obtained Google’s RGB images through the open-source QGIS software.

The dataset containing the locations and shapes of APGs was compiled through fieldwork, followed by the digitization of the collected data. The primary goal of the fieldwork was to ensure the precise identification and digitization of plastic greenhouses exclusively. Distinguishing between glass and plastic greenhouses from aerial imagery can be challenging due to their visual similarities. As a result, GPS-based localization was employed to accurately label plastic greenhouses during the training phase. Glass greenhouses typically exhibit higher reflectivity and transparency, while plastic greenhouses may vary in opacity and often develop textural changes over time. Consequently, field verification is crucial to accurately differentiate between these two types and ensure the reliability of the collected data.

A total of 3531 samples were collected, each representing an individual greenhouse polygon, including 1553 damaged and 1978 undamaged APG samples. The collection locations were digitized using QGIS software, which provides access to Google Earth imagery, enabling the creation of precise polygons for the study area and ensuring accuracy in labeling. Field validation was conducted by the authors through site visits to verify a representative subset of annotated greenhouses. Once the greenhouse shapes were accurately annotated, labeled masks were generated for training the proposed models. The first panel of Figure 1 illustrates the pipeline for location identification, digitization, and mask labeling. Each greenhouse is

[3] Earth Observation Satellite, Airbus
[4] Google Maps, Google Earth, and Street View Guidelines

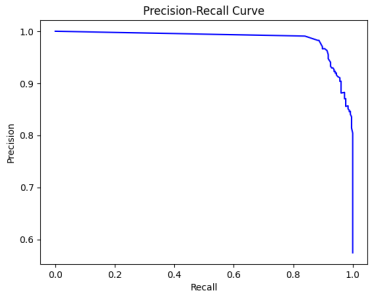

Figure 6. Precision-Recall curve for classification model

centered in the middle of a labeled mask, with its corresponding aerial image following the same alignment. This method helps the model learn a centralization pattern for each identified segment, which it can then use to distinguish plastic greenhouses from other structures, such as buildings. It is also worth noting that the substantial size of APGs greatly facilitates their detection, making it easier to distinguish them from surrounding structures. Moreover, a key aspect of the training strategy involved including images of buildings with constructions similar to APGs but with labeled masks uniformly set to 0 (Non-APGs), (See Figure 1, first panel).

2.1 Deep learning application

Deep learning, particularly through the use of CNNs, has significantly advanced the field of image processing, including segmentation [Shamsoshoara et al., 2021] and classification [Pan et al., 2020]. CNNs excel at learning patterns and features from images, allowing them to detect and classify objects accurately. Among the various architectures developed for image processing, U-Net stands out due to its efficacy in various applications, from biomedical [Ronneberger et al., 2015] to earth observation aerial images [Omarzadeh et al., 2024]. In this work, we employ a U-Net architecture with a MobileNetV2 backbone to classify damaged and undamaged APGs.

MobileNetV2 [Sandler et al., 2018] is a convolutional neural network specifically designed for execution on embedded devices that need to perform computer vision tasks. Embedded devices are small, specialized hardware systems such as smartphones, drones, or IoT sensors that have limited processing power, memory, and energy resources. This architecture was selected due to its effective balance between computational efficiency and performance, making it particularly suitable for tasks requiring robust feature extraction and classification in resource-constrained environments. It applies Depthwise Separable Convolutions (dsc) to reduce computation (Figure 4). MobileNetV2 has demonstrated significant performance in object detection, image classification, and segmentation tasks while maintaining highly memory-efficient inference.

In this study, “damaged” APGs are defined as plastic greenhouses with visible tears, holes, or deformations affecting structural integrity or coverage (Figure 3). An on-site verification was considered to ensure consistency between visual interpretation and actual structural conditions.

We use the YOLOv11 model in addition to MobileNetV2, which is one of the two most recent developments in the YOLO (You Only Look Once) series [Redmon et al., 2016]. This model is well-known for its remarkable speed, accuracy, and interpretability in object detection tasks. In order to

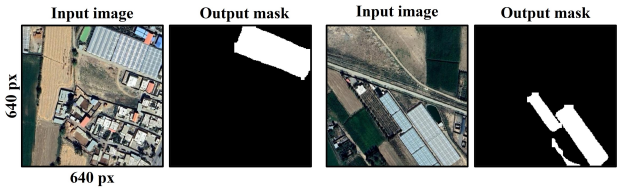

Figure 7. Segmentation of plastic greenhouses from 640×640 px satellite images. White regions in the masks accurately represent detected greenhouse structures, effectively distinguishing them from surrounding buildings and landscapes.

increase performance and usefulness, YOLOv11 introduces a number of novel architectural improvements while building on the strengths of its predecessors. The input, backbone, neck, and head are the four main parts of the model. The input component uses mosaic data augmentation to improve the robustness and quality of the images. The backbone integrates the C3K2 module, an optimized version of the Cross-Stage Partial (CSP) module with kernel size 2, which significantly improves feature extraction efficiency. Additionally, the C2PSA module [Wang et al., 2024] (Convolutional block with Parallel Spatial Attention), functioning similarly to an attention mechanism, is positioned after the Spatial Pyramid Pooling Fast (SPPF) layer [Dewi et al., 2022] to further refine feature representation. The neck section utilizes a combination of Feature Pyramid Network (FPN) and Path Aggregation Network (PAN) architectures, enabling effective multi-scale feature fusion and aggregation. Finally, using the enriched features that the neck provides, the head component carries out high-precision object detection, as shown in Figure 5. To focus on accurate and efficient object detection tasks, we use YOLOv11n (yolo11n-seg for the segmentation task) as the baseline model for our research due to its lightweight design and ability to be deployed in resource-constrained environments.

Together, MobileNetV2 and YOLOv11 provide a powerful combination for comprehensive image analysis, balancing efficiency and accuracy in our research framework. MobileNetV2 excels in classification tasks, while YOLOv11 enhances our ability to perform precise object detection and segmentation, ensuring robust and efficient analysis of visual data.

2.2 Data Augmentation

Data augmentation was applied extensively across both the segmentation and classification stages to increase the diversity of the training data and improve model robustness. For the segmentation task, YOLOv11 employed automatic augmentation through the Albumentations library [Buslaev et al., 2020]. This included preprocessing transformations such as blur, contrast enhancement, random erasing, and geometric augmentations like flipping and rotation. These augmentations allowed the model to handle variations in image quality and appearance, which are common in real-world remote sensing imagery.

For the classification task, online augmentation was applied dynamically during training. Techniques such as zooming, rotation, shearing, and horizontal and vertical flipping generated new variations of each input image in real time. Mosaic augmentation was also incorporated to further expand the diversity of visual patterns encountered during training. A 0.15 validation split ensured that model evaluation remained unbiased.

Data augmentation plays a vital role in enhancing machine learning models, especially when training data is limited [Alif, 2024, Maharana et al., 2022]. Artificially expanding the dataset helps prevent overfitting and enables models to recognize patterns across a wider range of conditions [Shorten and Khoshgoftaar, 2019]. By introducing realistic geometric and appearance-based variations, the applied augmentations improved the generalization capability of both YOLOv11 and the classification network. This led to gradual improvements in precision, recall, and mAP50 across training epochs, demonstrating the effectiveness of augmentation in producing more reliable and adaptable models for practical applications.

Set	Total Samples	Undamaged APGs	Damaged APGs	F1 Score
1	150	100	50	0.758
2	200	100	100	0.765
3	150	50	100	0.952
Average	——	——	——	**0.825**

Table 1. Testing F1 score across balanced and imbalanced datasets.

County	Predicted Area (km²)	Officially Reported Area (km²)
Varamin	3.98	5.22
Pakdasht	6.77	15.43
Pishva	7.33	14.00
Qarchak	6.50	10.00

Table 2. Comparison of Predicted APG Areas and Officially Reported Greenhouse Areas (km²) Across Counties. The official data includes both plastic and glass greenhouses.

For the classification task, model performance was assessed using Precision, Recall, and F1 Score, which are particularly informative under class imbalance conditions [Gevaert and Belgiu, 2022]:

$$\text{Precision} = \frac{TP}{TP + FP}$$

$$\text{Recall} = \frac{TP}{TP + FN}$$

$$\text{F1} = 2 \times \frac{\text{Precision} \times \text{Recall}}{\text{Precision} + \text{Recall}}$$

Figure 6 illustrates the precision–recall curve for our classification model. The curve shows consistently high precision across a wide range of recall values, indicating stable performance and good generalization to unseen samples.

2.3 Accuracy Assessment Metrics

The segmentation performance was evaluated using the Jaccard Index, also known as Intersection over Union (IoU) [Yuan et al., 2017], defined as:

$$J(M, C) = \frac{|M \cap C|}{|M| + |C| - |M \cap C|}$$

where M and C denote the ground truth and predicted masks, respectively. $J(M, C)$ ranges between 0 and 1, with higher values indicating better overlap between the predicted and reference areas. This metric is widely used for segmentation evaluation in both medical and remote sensing imagery [Setiawan, 2020, Muhadi et al., 2020].

To ensure a fair evaluation, the dataset was divided into four test sets with varying ratios of damaged and undamaged APGs, simulating both balanced and imbalanced real-world conditions. F1

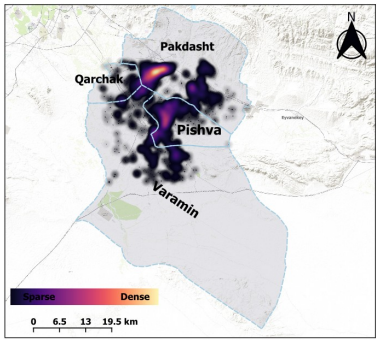

Figure 8. Spatial distribution of APGs

scores were computed separately for each set, as reported in Table 1. This multi-split evaluation provides a more reliable estimate of model performance under different class distributions and reduces the risk of overfitting to a single data composition. The mean F1 score across all test sets reached 0.825, reflecting the model’s robustness in distinguishing damaged structures despite data imbalance.

Furthermore, the model achieved an overall classification accuracy of 90.77% when predictions were compared with ground truth labels. While accuracy provides a general measure of correctness, the F1 score offers a more balanced evaluation under class imbalance, balancing precision and recall. By combining accuracy, F1 score, and the precision–recall relationship, we comprehensively validate the classifier’s ability to identify damaged greenhouses across varying sample distributions. These results highlight the model’s applicability for large-scale environmental monitoring and damage detection in heterogeneous agricultural landscapes.

3. Results

The first step involved generating binary segmentation masks (1 = APG, 0 = background) from 0.5-meter imagery using the YOLOv11 model. Figure 7 shows sample segmentation outputs, demonstrating the accurate delineation of APG structures and clear separation from buildings and other agricultural features.

Across the four counties (Varamin, Qarchak, Pishva, and Pakdasht), a total of 158,912 image tiles (640 × 640 px) were processed. Among these, 6,835 tiles were identified as containing APGs, and their corresponding masks were retained for further analysis. The total mapped APG area derived from these segmentation masks is 18.73 km^2 (Table 2).

Figure 8 illustrates the spatial distribution of detected greenhouses. The highest densities occur in the northwestern (Pakdasht) and central (Pishva) regions, while southern areas show minimal greenhouse presence due to arid conditions and distance from major population centers.

To contextualize the segmentation-derived area estimates, we compared our results with the 2024 report from the Varamin County Agricultural Organization. This report states that the total greenhouse area in Varamin, combining plastic and glass structures, covers 5.22 km^2. In comparison, our method identifies 3.98 km^2 of plastic-only greenhouses in the same region. This close agreement supports the reliability of our segmentation model and highlights its practical utility in estimating

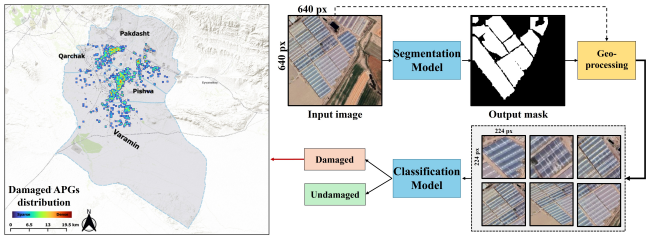

Figure 9. Classification data preparation and the distribution of damaged APGs in the area.

plastic greenhouse areas, despite the exclusion of glass greenhouses.

In the next step, segmentation outputs were used to guide the classification of damaged APGs. Each segmented greenhouse was enclosed in a bounding box, cropped, and resized to 224 pixels before being used as classification input. This workflow is illustrated in Figure 9.

The classification model identified 1,863 damaged APGs across the study area. Field verification was performed on 20% of the results. Their spatial distribution (shown in Figure 9) reveals that most damaged structures are concentrated in the central and northwestern regions. Figure 3 presents sample images of damaged APGs considered in this study.

Table 1 summarizes the model performance using three separate test sets with varying class balance. The model achieved an average F1 score of 0.825, which is comparable to and in some cases exceeds performance reported in recent APG damage-detection studies based on lightweight CNNs and U-Net variants. Importantly, all test sets included images that the model had never seen during training, demonstrating its ability to generalize to new data within the study region. While greenhouse structures across Iran often share similar shapes and materials, suggesting the model’s potential applicability to other regions, slight design or environmental differences may require minimal fine-tuning using a small number of samples from the new area to maintain high performance.

Training and validation curves for the classifier are shown in Figure 11. Both loss and accuracy exhibit stable and consistent trends, demonstrating effective training and generalization with no indication of overfitting. These results indicate that the model is robust across both balanced and imbalanced datasets, supporting its application for large-scale environmental monitoring.

4. Discussion and Conclusions

The integration of YOLOv11-seg and MobileNetV2 demonstrates that very high-resolution RGB imagery can effectively support both detection and condition assessment of agricultural plastic greenhouses (APGs). Our findings confirm a growing spatial footprint of greenhouse farming across Tehran County and reveal concentrated clusters of damaged structures, particularly in Pakdasht and Pishva. These patterns align with government statistics[5] and Sentinel-2 imagery from 2021–2024 (Table 2 and Figure 10), indicating a regional shift toward greenhouse-based cultivation as open-field farming declines.

Few studies have simultaneously addressed APG segmentation and structural damage classification using very high-resolution

[5] Agricultural Jihad Organization of Varamin County

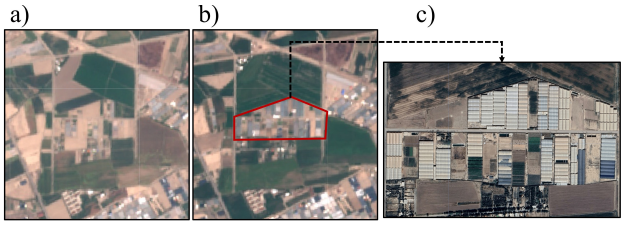

Figure 10. Detected transformations in land use: (a) Sentinel-2, 2021, 10 m resolution; (b) Sentinel-2, 2024, 10 m resolution; and (c) Google Earth, 0.5 m resolution confirming the presence of plastic greenhouses in the area.

imagery. Previous works either focused solely on greenhouse detection [Song et al., 2025] or used medium-resolution imagery insufficient for assessing structural integrity [Acharki et al., 2024]. In contrast, our approach leverages 0.5 m imagery, enabling detection of features as small as 10 × 10 m and facilitating identification of damaged structures. By combining segmentation with damage classification, the framework provides a more comprehensive assessment linking agricultural productivity with environmental risks, including plastic waste accumulation.

Despite these strengths, several limitations should be noted. Damage classification was validated visually, rather than with fully quantifiable ground-truth data, as no official dataset exists for this region. While visual inspection provides preliminary verification, it introduces subjectivity and may miss subtle forms of structural degradation. Field inspections to enhance the reliability of the labels were conducted (roughly one-fifth of the mapped greenhouses), enabling hands-on verification of the physical characteristics of the structures. Future research should include structured field surveys, drone-based monitoring, or collaboration with local agricultural authorities to generate reliable ground-truth data. Additionally, relying solely on RGB imagery limits spectral sensitivity for distinguishing materials or subtle damage, which could be improved using multispectral, thermal, or LiDAR data. While the model was trained and tested only on the Tehran County dataset, the relatively standardized design of plastic greenhouses across Iran suggests potential applicability in other regions. Minor variations in greenhouse construction or environmental conditions could be addressed by fine-tuning the model with a small number of local samples, allowing transferability without retraining from scratch.

The practical implications of this work are significant. Accurate mapping of greenhouse locations enables estimation of cultivated area, potential crop yield, and land-use change monitoring, supporting evidence-based agricultural planning. Identification of damaged APGs informs targeted maintenance and plastic waste management, helping prioritize cleanup efforts and mitigate environmental impacts. Moreover, the framework can aid climate-resilience planning by monitoring greenhouses vulnerable to extreme weather events, supporting disaster preparedness and post-event recovery strategies. These results provide a validated, scalable framework that can guide agricultural management and environmental monitoring, while also being adaptable to similar greenhouse regions with minimal additional effort.

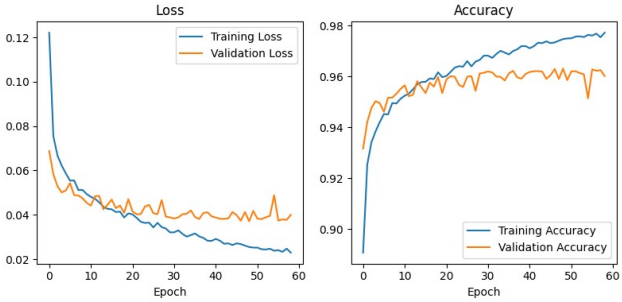

Figure 11. Training and validation loss and accuracy curves for the classification model.

Acknowledgment

This publication has emanated from research conducted with the financial support of Taighde Éireann Research Ireland under Grant number 18/CRT/6183.

References

Acharki, S., Veettil, B. K., Vizzari, M., 2024. Plastic-covered greenhouses mapping in Morocco with Google Earth engine: Comparing Sentinel-2 and Landsat-8 data using pixel-and object-based methods. *Remote Sensing Applications: Society and Environment*, 34, 101158.

Alif, M. A. R., 2024. Yolov11 for vehicle detection: Advancements, performance, and applications in intelligent transportation systems. *arXiv preprint arXiv:2410.22898*.

Baudoin, W., Von Zabeltitz, C., 2001. Greenhouse constructions for small scale farmers in tropical regions. *International Symposium on Design and Environmental Control of Tropical and Subtropical Greenhouses 578*, 171–179.

Buslaev, A., Iglovikov, V. I., Khvedchenya, E., Parinov, A., Druzhinin, M., Kalinin, A. A., 2020. Albumentations: fast and flexible image augmentations. *Information*, 11(2), 125.

Chen, W., Xu, Y., Zhang, Z., Yang, L., Pan, X., Jia, Z., 2021. Mapping agricultural plastic greenhouses using Google Earth images and deep learning. *Computers and Electronics in Agriculture*, 191, 106552.

Chen, Z., Zhang, T., Ouyang, C., 2018. End-to-end airplane detection using transfer learning in remote sensing images. *Remote Sensing*, 10(1), 139.

Dewi, C., Chen, R.-C., Jiang, X., Yu, H., 2022. Deep convolutional neural network for enhancing traffic sign recognition developed on Yolo V4. *Multimedia Tools and Applications*, 81(26), 37821–37845.

Duhl, T. R., Guenther, A., Helmig, D., 2012. Estimating urban vegetation cover fraction using Google Earth® images. *Journal of Land Use Science*, 7(3), 311–329.

Feizizadeh, B., Lakes, T., Omarzadeh, D., Sharifi, A., Blaschke, T., Karimzadeh, S., 2022a. Scenario-based analysis of the impacts of lake drying on food production in the Lake Urmia Basin of Northern Iran. *Scientific reports*, 12(1), 6237.

Feizizadeh, B., Omarzadeh, D., Mohammadzadeh Alajujeh, K., Blaschke, T., Makki, M., 2022b. Impacts of the urmia lake

drought on soil salinity and degradation risk: An integrated geoinformatics analysis and monitoring approach. remote sens. 2022, 14, 3407.

Feng, Q., Niu, B., Chen, B., Ren, Y., Zhu, D., Yang, J., Liu, J., Ou, C., Li, B., 2021. Mapping of plastic greenhouses and mulching films from very high resolution remote sensing imagery based on a dilated and non-local convolutional neural network. *International Journal of Applied Earth Observation and Geoinformation*, 102, 102441.

Gaetano, R., Ienco, D., Ose, K., Cresson, R., 2018. A two-branch CNN architecture for land cover classification of PAN and MS imagery. *Remote Sensing*, 10(11), 1746.

Gevaert, C. M., Belgiu, M., 2022. Assessing the generalization capability of deep learning networks for aerial image classification using landscape metrics. *International Journal of Applied Earth Observation and Geoinformation*, 114, 103054.

Gündoğdu, R., Önder, D., Gündoğdu, S., Gwinnett, C., 2022. Plastics derived from disposable greenhouse plastic films and irrigation pipes in agricultural soils: a case study from Turkey. *Environmental Science and Pollution Research*, 29(58), 87706–87716.

Jakab, B., van Leeuwen, B., Tobak, Z., 2021. Detection of Plastic Greenhouses Using High Resolution Rgb Remote Sensing Data and Convolutional Neural Network. *Journal of Environmental Geography*, 14(1-2), 28–46.

Koc-San, D., 2013. Evaluation of different classification techniques for the detection of glass and plastic greenhouses from WorldView-2 satellite imagery. *Journal of Applied Remote Sensing*, 7(1), 073553–073553.

Levin, N., Lugassi, R., Ramon, U., Braun, O., Ben-Dor, E., 2007. Remote sensing as a tool for monitoring plasticulture in agricultural landscapes. *International journal of remote sensing*, 28(1), 183–202.

Maharana, K., Mondal, S., Nemade, B., 2022. A review: Data pre-processing and data augmentation techniques. *Global Transitions Proceedings*, 3(1), 91–99.

Mboga, N., Grippa, T., Georganos, S., Vanhuysse, S., Smets, B., Dewitte, O., Wolff, E., Lennert, M., 2020. Fully convolutional networks for land cover classification from historical panchromatic aerial photographs. *ISPRS Journal of Photogrammetry and Remote Sensing*, 167, 385–395.

Muhadi, N. A., Abdullah, A. F., Bejo, S. K., Mahadi, M. R., Mijic, A., 2020. Image segmentation methods for flood monitoring system. *Water*, 12(6), 1825.

Omarzadeh, D., González-Godoy, A., Bustos, C., Martín-Fernández, K., Scotto, C., Sánchez, C., Lapedriza, A., Borge-Holthoefer, J., 2024. Explainable Automatic Detection of Fiber–Cement Roofs in Aerial RGB Images. *Remote Sensing*, 16(8), 1342.

Pan, Z., Xu, J., Guo, Y., Hu, Y., Wang, G., 2020. Deep learning segmentation and classification for urban village using a worldview satellite image based on U-Net. *Remote Sensing*, 12(10), 1574.

Pirbasti, M. A., McArdle, G., Akbari, V., 2024. Hedgerows Monitoring in Remote Sensing: A Comprehensive Review. *IEEE Access*, 12, 156184-156207.

Ploton, P., Pélissier, R., Proisy, C., Flavenot, T., Barbier, N., Rai, S., Couteron, P., 2012. Assessing aboveground tropical forest biomass using Google Earth canopy images. *Ecological Applications*, 22(3), 993–1003.

Qamar, F., Dobler, G., 2020. Pixel-wise classification of high-resolution ground-based urban hyperspectral images with convolutional neural networks. *Remote Sensing*, 12(16), 2540.

Redmon, J., Divvala, S., Girshick, R., Farhadi, A., 2016. You only look once: Unified, real-time object detection. *Proceedings of the IEEE conference on computer vision and pattern recognition*, 779–788.

Ronneberger, O., Fischer, P., Brox, T., 2015. U-net: Convolutional networks for biomedical image segmentation. *Medical image computing and computer-assisted intervention–MICCAI 2015: 18th international conference, Munich, Germany, October 5-9, 2015, proceedings, part III 18*, Springer, 234–241.

Ruel, M. T., Garrett, J., Yosef, S., Olivier, M., 2017. Urbanization, food security and nutrition. *Nutrition and health in a developing world*, 705–735.

Sandler, M., Howard, A., Zhu, M., Zhmoginov, A., Chen, L.-C., 2018. Mobilenetv2: Inverted residuals and linear bottlenecks. *Proceedings of the IEEE conference on computer vision and pattern recognition*, 4510–4520.

Setiawan, A. W., 2020. Image segmentation metrics in skin lesion: accuracy, sensitivity, specificity, dice coefficient, jaccard index, and matthews correlation coefficient. *2020 International Conference on Computer Engineering, Network, and Intelligent Multimedia (CENIM)*, IEEE, 97–102.

Shamsoshoara, A., Afghah, F., Razi, A., Zheng, L., Fulé, P. Z., Blasch, E., 2021. Aerial imagery pile burn detection using deep learning: The FLAME dataset. *Computer Networks*, 193, 108001.

Shi, L., Huang, X., Zhong, T., Taubenböck, H., 2019. Mapping plastic greenhouses using spectral metrics derived from GaoFen-2 satellite data. *IEEE Journal of Selected Topics in Applied Earth Observations and Remote Sensing*, 13, 49–59.

Shi WeiMing, S. W., Yao Jing, Y. J., Yan Feng, Y. F., 2009. Vegetable cultivation under greenhouse conditions leads to rapid accumulation of nutrients, acidification and salinity of soils and groundwater contamination in South-Eastern China.

Shorten, C., Khoshgoftaar, T. M., 2019. A survey on image data augmentation for deep learning. *Journal of big data*, 6(1), 1–48.

Song, W., He, H., Dai, J., Jia, G., 2025. Extraction of agricultural plastic greenhouses based on a U-Net convolutional neural network coupled with edge expansion and loss function improvement. *Journal of the Air & Waste Management Association*, 75(2), 109–120.

Stewart, C., Lazzarini, M., Luna, A., Albani, S., 2020. Deep learning with open data for desert road mapping. *Remote Sensing*, 12(14), 2274.

Sun, H., Wang, L., Lin, R., Zhang, Z., Zhang, B., 2021. Mapping plastic greenhouses with two-temporal sentinel-2 images and 1d-cnn deep learning. *Remote Sensing*, 13(14), 2820.

Tong, X., Zhang, X., Fensholt, R., Jensen, P. R. D., Li, S., Larsen, M. N., Reiner, F., Tian, F., Brandt, M., 2024. Global area boom for greenhouse cultivation revealed by satellite mapping. *Nature Food*, 1–11.

Wang, C.-Y., Yeh, I.-H., Mark Liao, H.-Y., 2024. Yolov9: Learning what you want to learn using programmable gradient information. *European conference on computer vision*, Springer, 1–21.

Yang, D., Chen, J., Zhou, Y., Chen, X., Chen, X., Cao, X., 2017. Mapping plastic greenhouse with medium spatial resolution satellite data: Development of a new spectral index. *ISPRS Journal of Photogrammetry and Remote Sensing*, 128, 47–60.

Yuan, Y., Chao, M., Lo, Y.-C., 2017. Automatic skin lesion segmentation using deep fully convolutional networks with jaccard distance. *IEEE transactions on medical imaging*, 36(9), 1876–1886.

https://doi.org/10.5194/isprs-annals-XI-4-2026-53-2026